

Received 20 January 2025, accepted 10 February 2025, date of publication 18 February 2025, date of current version 24 February 2025.

Digital Object Identifier 10.1109/ACCESS.2025.3543323

## RESEARCH ARTICLE

# Inferring Urban Air Temperatures From Land Surface Temperatures With the E3SM Land Model (uELM), Satellite Observations, and Measurement Campaign

JANGHO LEE 

Department of Earth and Environmental Sciences, University of Illinois Chicago, Chicago, IL 60607, USA

e-mail: jholee@uic.edu

This work was supported by U.S. Department of Energy, Office of Science, Office of Biological and Environmental Research's Urban Integrated Field Laboratories CROCUS Project Research Activity under Award DE-SC0023226.

**ABSTRACT** This study investigates how urban land-cover variability—from dense built areas to predominantly vegetated neighborhoods—affects the relationship between land surface temperature (LST) and near-surface air temperature (T2M) using an ultrahigh-resolution land model (uELM). 125 simulations adjusting fractions of urban vs. vegetation, mid-rise vs. low-rise buildings and tree vs. lawn cover reveal strong LST–T2M coupling, as well as its dependency on land cover and diurnal variations. These physics-based findings support a machine-learning, inverse-modeling approach, training a XGBoost algorithm on simulated LST–T2M pairs to estimate T2M from satellite-based LST. Applied to the Chicago region with GOES-16 data and compared against vehicle-based measurements, the model and measurements agrees relatively well midday but shows evening mismatches tied to uneven cooling and hyperlocal factors during observation. Despite these discrepancies, blending mechanistic modeling with data-driven inversion has potential to refine urban T2M estimates, informing heat mitigation strategies and advancing urban climate research.

**INDEX TERMS** Climate model, land model, E3SM, ELM, uELM, urban, air temperature, land surface temperature, satellite, remote sensing, measurement campaign.

## I. INTRODUCTION

As global warming accelerates, the impacts of rising global temperatures are increasingly evident across various aspects of the climate system. These include more severe and frequent hurricanes, extreme heat events, intensified precipitation, flooding, and prolonged droughts. Among these, extreme heat events stand out as one of the most direct and observable consequences of climate change. In this context, accurate estimates of urban near-surface air temperature, or 2-m air temperature (T2M) are crucial for a variety of urban applications—including public health surveillance during heat waves [1], [2], [3], energy-demand forecasting [4],

[5], [6], [7], and infrastructure management [8], [9]—all of which are exacerbated by the urban heat island (UHI) effect. As global urbanization accelerates, cities are rapidly expanding, altering land cover in ways that amplify local heat retention and reduce natural cooling [10], [11], [12], [13]. Despite its importance, T2M monitoring in urban environments remains limited. While meteorological stations provide reliable point measurements, their coverage in dense urban cores is often sparse, leaving critical data gaps in regions with varied building densities, impervious surfaces, and anthropogenic heat sources. Mobile or vehicle-based sensors can enhance data density but are costly and logistically challenging to maintain at scale over extended periods.

In contrast, land surface temperature (LST) data are often more available at higher spatial and temporal resolutions,

The associate editor coordinating the review of this manuscript and approving it for publication was Stefania Bonafoni .

especially from satellites. The Geostationary Operational Environmental Satellite (GOES-R) series, for instance, retrieves hourly LST over North America at 2 km resolution [14], [15]. Meanwhile, the Moderate Resolution Imaging Spectroradiometer (MODIS) onboard NASA's Terra and Aqua satellites provides near-global coverage at around 1 km resolution [16], [17], generally revisiting a given location two times per day. Despite this rich availability of LST data, translating it to T2M remains nontrivial, and it has been an interest to multiple previous studies [18], [19], [20], [21], [22]. T2M is measured approximately 2 m above ground and shaped by boundary-layer dynamics and materials near the surface, whereas LST quantifies the skin temperature of the land surface itself. These discrepancies can be more significant in urban areas, where factors such as building geometry, vertical mixing, and localized heat storage can cause substantial deviations between surface and near-surface temperatures. Consequently, although LST and T2M are correlated, their direct linkage often requires further modeling to account for the complex nuances of urban environments.

In response to address this gap, previous studies have used an approach that pairs satellite-derived LST with ground-based T2M measurements to build statistical models [23], [24], [25], often powered by machine-learning or deep-learning architectures such as Long-Short Term Memory (LSTM) [26], [27], [28] or other types of Recurrent Neural Networks (RNN) [29], [30]. Once trained, these models can rapidly and inexpensively infer T2M from LST over extensive spatial domains. However, their performance depends on the quality and distribution of meteorological stations, which are frequently uneven and subject to urban-rural biases of their placements. Moreover, many of these purely empirical methods struggle to incorporate or represent the physical processes underlying surface-atmosphere exchanges.

Another method relies on high-resolution regional climate models, often specifically adapted for urban areas, such as Weather Research and Forecasting Urban (WRF-Urban) model [31], [32] or The Community Land Model-Urban (CLMU) [33], [34], [35]. These physics-based models offer a physically consistent output of meteorological variables—unlike purely empirical methods—and include explicit representations of surface energy budgets and urban canopy effects. However, running such models at fine spatial resolutions comes with high computational demands, and their performance can be limited by the quality of lower-scale atmospheric forcing data. Additionally, these urban-resolving models parameterize the urban structure—meaning that they rely on simplified treatments or assumptions regarding building geometry, street canyon width, wall-to-roof ratios, or anthropogenic heat sources to approximate complex urban realities [31], [33], [36]. While this can result in discrepancies between simulated and observed urban microclimates, these physics-based approaches remain valuable for elucidating key dynamics of how built infrastructure interacts with the

atmosphere, especially when supplemented with observational or data-driven methods.

This study employs an ultrahigh-resolution version of the Energy Exascale Earth System Model (E3SM) Land Model (uELM) [37], [38], [39] to systematically investigate how different urban land-cover configurations—from dense urban built area to predominantly vegetated neighborhoods—govern the relationship between LST and T2M. Unlike approaches that rely strictly on statistically matching station-based T2M to satellite LST, uELM incorporates realistic representations of energy, moisture, and momentum exchange at the land-atmosphere interface. By forcing uELM with a diverse set of urban fractions and analyzing the resulting LST outputs, this study builds a rich catalog of T2M-LST interactions, capturing the complex thermal dynamics driven by varying land-cover conditions. I then train a machine-learning model on these uELM outputs to estimate T2M from LST, thereby creating a hybrid framework that retains physical realism while remaining computationally efficient.

To illustrate the potential of this method, I apply it to the Chicago metropolitan region using GOES-16 satellite LST data at 2 km resolution. In addition to investigating how land-cover variability affects LST-T2M coupling—and how these insights can refine urban T2M estimates—I also compare the resulting T2M fields with vehicle-based measurements to compare the results with other data source. This is particularly important for the city of Chicago, because Chicago, as one of the largest and most densely populated urban centers in the United States, exhibits significant diversity in building heights, street layouts, vegetation cover, and anthropogenic heat sources. Overall, by systematically incorporating land-cover heterogeneity into a physics-based framework, this study demonstrates a more robust understanding of the LST-T2M relationship.

The novelty of this work lies in using uELM to explore the LST-T2M relationship, augmenting a physics-based land model with a machine-learning inversion, and integrating multiple data sources—including GOES-16 satellite retrievals and vehicle-based measurements. This combined approach bridges the gap between purely empirical models and highly complex regional simulations, while also demonstrating potential for multiple practical applications. The framework provides a systematic path to extend satellite-based T2M retrievals to cities worldwide—particularly those with minimal meteorological networks—thereby improving urban heat risk assessments and informing adaptation strategies for a warming climate.

## II. DATA

### A. SATELLITE-BASED LAND SURFACE TEMPERATURE

Satellite-based temperature observations for this study come from the Geostationary Operational Environmental Satellite-16 (GOES-16). GOES-16 carries the Advanced Baseline Imager (ABI), which provides hourly land surface temperature (LST) estimates over the eastern United States at a

nominal 2 km spatial resolution. This study specifically focuses on GOES-16 retrievals collected on July 28, 2023, covering the metropolitan Chicago region.

Prior intercomparisons report that the typical GOES-16 LST retrieval has an error margin below 2 K [14], [40]. These LST products are derived by applying atmospheric corrections, cloud masking, and surface emissivity adjustments to thermal-infrared observations from the ABI. Since each GOES-16 LST value represents an average of the surface temperature across a 2 Km grid cell, I overlay the satellite grid on the Chicago metropolitan area (Figure 1a). Figures 1b and 1c provide examples of GOES-16 LST fields at 3–4 pm (afternoon, AF) and 7–8 pm (evening, PM), respectively. Although GOES-16 also provides data during the early morning, cloud contamination at 6–7 AM precludes reliable retrievals for that period.

**B. VEHICLE-BASED AIR TEMPERATURE**

A second source of temperature data comes from the NOAA Heat-Watch campaign, conducted on the same date (July 28, 2023). During this campaign, 100 vehicles were equipped with calibrated temperature sensors to measure near-surface air temperature (T2M). The vehicles drove across diverse neighborhoods in the metropolitan Chicago region at three designated times—6–7 AM (AM), 3–4 pm (AF), and 7–8 pm (PM)—in order to capture the diurnal variability of T2M. Data collection protocols typically include high-frequency logging of temperature and precise GPS coordinates, enabling spatially detailed temperature mapping. About 140k measurement were made during each period.

Since GOES-16 LST retrievals at 6–7 AM are compromised by cloud cover, this analysis focuses on the AF and PM periods, which coincide with clear-sky conditions in the satellite data. Figures 1d and 1e show the vehicle routes during the AF and PM periods, where white lines trace the paths of the mobile sensors. To compare these in situ observations with the GOES-16 LST, I spatially aggregate the vehicle-based T2M data within each 2 Km GOES-16 grid cell. Specifically, all T2M measurements falling inside a given satellite pixel during the relevant one-hour window (3–4 pm or 7–8 pm) are averaged to produce a single near-surface air temperature value per cell. This procedure ensures direct comparability between the satellite-derived LST and the mean T2M from the mobile campaign.

**C. URBAN LAND COVER INFORMATION**

Beyond the temperature variables, land-cover information for Chicago at a 2 Km resolution is generated by merging two primary datasets: the building footprints from the Chicago Data Portal and the high-resolution Coastal Change Analysis Program (C-CAP) regional land cover from NOAA [41]. Both datasets are re-projected and clipped to the same coordinate reference system and study area boundaries to ensure accurate spatial alignment.

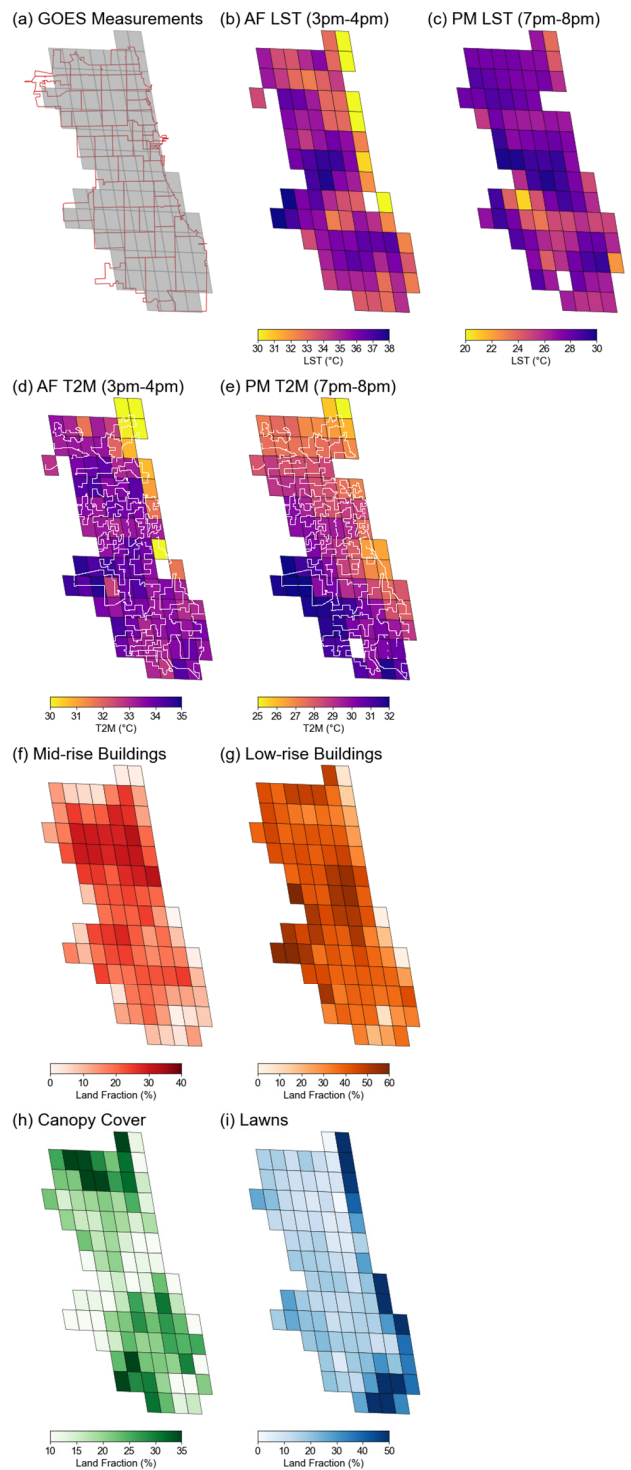


**FIGURE 1.** (a) Map of zip codes in the Chicago area (outlined in red) with the GOES-16 grid represented in gray. (b) GOES-16 LST (°C) retrieved between 3–4 pm local time on July 28, 2023. (c) Same as (b), but for 7–8 pm. (d) Aggregated T2M (°C) from the vehicle-based campaign during 3–4 pm, with the measurement routes shown in white. (e) Same as (d), but for 7–8 pm. (f) Land-cover fraction of mid-rise buildings, aggregated to the GOES-16 grid. (g–i) Same as (f), but for low-rise buildings, canopy cover, and lawns, respectively.

The building footprints dataset provides polygons outlining each structure along with information on the number

of floors. A floor-count threshold is applied to classify each building as either mid-rise or low-rise. These building polygons are then overlaid onto the impervious surface classification derived from the C-CAP product, which is based on 1 m lidar and satellite imagery. Polygons that intersect with the impervious class are explicitly labeled as buildings, ensuring that other impervious surfaces, such as roads and parking lots, are distinctly categorized as non-building urban areas.

Tree coverage is directly identified using the canopy classification from C-CAP and retained as a separate category. Any remaining areas not classified as buildings, non-building impervious surfaces, or water bodies are categorized as lawns. The reconciled land-cover data, combining the building footprints with the C-CAP classifications, is then aggregated to a 2 Km grid. Fractional coverage of each category—mid-rise buildings, low-rise buildings, trees, and lawns—is calculated within each grid cell by summing the polygon areas (for buildings) or pixel counts (for C-CAP) and dividing by the total cell area. This process yields a detailed and refined land-cover composition for every 2 Km cell in the domain.

The final maps, shown in Figures 1f–1i, depict the spatial distribution of these four categories and highlight the heterogeneity of Chicago’s urban landscape, offering a valuable foundation for understanding how land-cover variability influences thermal dynamics at the local scale.

### III. METHOD OF ANALYSIS

#### A. uELM OVERVIEW

This study utilizes the ultrahigh-resolution E3SM Land Model (uELM), which operates at a 1 Km  $\times$  1 Km spatial resolution. This high resolution is intended to capture the small-scale heterogeneity of land surfaces, making the model particularly well suited for studying the complex urban environments of large metropolitan areas like Chicago.

The underlying urban parameterization in uELM follows the same urban canyon framework that the Community Land Model (CLM) and its urban extension (CLMU) implement within the Community Earth System Model (CESM2). At the core of this parameterization is the “urban canyon” concept, which represents cityscapes as infinitely long canyons consisting of five key facets: building roofs, impervious canyon floors, pervious canyon floors, sunlit walls, and shaded walls. Although this framework abstracts the detailed geometry of real cities, it effectively captures the thermodynamic and radiative processes that drive urban microclimates.

Key parameters for each urban facet include morphological characteristics such as the canyon height-to-width ratio, radiative properties such as albedo and emissivity, and thermal attributes such as heat capacity and thermal conductivity (Table 1). By adopting this modeling strategy, uELM ensures consistency with established community models that use a comparable urban scheme, which facilitates integration with

other climate and weather models and leverages previous evaluation efforts.

#### B. uELM SIMULATION SETUP

uELM simulations are forced with seven meteorological variables: precipitation, solar radiation, longwave radiation, surface air pressure, air temperature, humidity, and wind speed. Following previous studies [37], [38], the meteorological inputs primarily come from the Daymet dataset, which offers daily data at high spatial resolution across North America. To ensure realistic subdaily variations, these daily values are downscaled to three-hourly intervals using the GSWP3 (Global Soil Wetness Project Phase 3) reanalysis. Although the model is nominally set up for Chicago at approximately 41.99° N, –87.74° E, these coordinates are less crucial for the present experiment because the same atmospheric forcing is applied across all scenarios, thereby isolating the effects of land-cover changes from meteorological differences.

The simulations begin in 1850 and run in transient mode through 2014, capturing changes in both atmospheric composition and land surface states. After completing the transient phase, output is extracted for July and August over the most recent 14-year span (2001–2014), a period selected because these months usually see the highest temperatures in Chicago. At this stage, this study systematically vary land-cover fractions within the 1 Km  $\times$  1 Km domain to explore how different levels of urbanization and vegetation affect near-surface climate. In particular, five levels of urban fraction are defined, ranging from 10 % to 90 %, and each urban fraction is further partitioned into mid-rise and low-rise building types in five increments (details in Table 1). The vegetated portion is also subdivided in five steps, split between trees (broadleaf deciduous temperate) and lawns (C3 irrigated). Because urban fraction, building type, and vegetation type each vary over five levels, this yields 125 total configurations (5  $\times$  5  $\times$  5). Identical meteorological forcing is used in all simulations, making it possible to evaluate how changes in building coverage and vegetation influence simulated LST and T2M.

#### C. HYBRID T2M ESTIMATION FROM LST

Building on the 28-month uELM simulation dataset—spanning July and August from 2001 to 2014 across 125 distinct land-cover configurations—a data-driven model is developed to predict T2M based on land surface temperature LST, fractional land-cover attributes (mid-rise buildings, low-rise buildings, trees, and lawns), and the hour of the day. This 28-month dataset, which is composed of 14 years of two-month (July and August) periods simulated under systematically varied urban–rural compositions, provides a broad spectrum of potential surface conditions in terms of morphology, thermal properties, and diurnal dynamics. The fundamental goal is to capture enough variability in surface characteristics and daily radiative cycles so that the derived

**TABLE 1.** Urban morphological, radiative, and thermal parameter for the mid-rise and low-rise building in this study.

Variable	Mid-rise Building	Low-rise Building	Unit
Canyon height to width ratio	1.60	0.48	Unitless
Emissivity of impervious road	0.88	0.91	Unitless
Emissivity of pervious road	0.95	0.95	Unitless
Emissivity of roof	0.64	0.48	Unitless
Emissivity of wall	0.92	0.89	Unitless
Height of roof	40	12	m
Thickness of roof	0.19	0.19	m
Thickness of wall	0.31	0.31	m
Height of wind in canyon	20	6	m
Fraction of roof	0.6	0.35	Unitless
Fraction of pervious road	0.375	0.69	Unitless
Direct albedo of impervious road	0.23	0.13	Unitless
Diffuse albedo of impervious road	0.23	0.13	Unitless
Direct albedo of pervious road	0.08	0.08	Unitless
Diffuse albedo of pervious road	0.23	0.13	Unitless
Direct albedo of roof	0.33	0.37	Unitless
Diffuse albedo of roof	0.33	0.37	Unitless
Direct albedo of wall	0.34	0.28	Unitless
Diffuse albedo of wall	0.34	0.28	Unitless
Thermal conductivity of roof	1.24	1.30	W/m·K
Thermal conductivity of wall	1.16	1.16	W/m·K
Thermal conductivity of impervious road	1.90	1.67	W/m·K
Volumetric heat capacity of roof	585559	594379	J/m <sup>3</sup> ·K
Volumetric heat capacity of wall	913189	875185	J/m <sup>3</sup> ·K
Volumetric heat capacity of impervious road	2100000	2060471	J/m <sup>3</sup> ·K

model can robustly “reverse-engineer” T2M from LST in real-world urban scenarios.

To achieve this, the eXtreme Gradient Boosting (XGBoost) algorithm [42] is employed. XGBoost is well known for its capacity to model complex, nonlinear interactions in regression tasks. Each training sample in the dataset consists of a specific hour, a combination of land-cover fractions (mid-rise, low-rise, trees, and lawns), and the uELM-simulated LST value, with the corresponding uELM T2M serving as the target variable. Representing hour as a feature allows the model to account for diurnal heating and cooling cycles, which heavily influence the LST–T2M relationship in urban environments. The data preparation involves reformatting 3-hourly model outputs so that each 125-scenario simulation contributes a 3-hourly time series over the 28-month window, ultimately generating a large set of features–target pairs (total of 1,288,000 samples).

Hyperparameter tuning of the XGBoost model is performed via Bayesian optimization, which iteratively refines its search space for parameters such as learning rate, maximum tree depth, and minimum child weight. At each iteration, a range of candidate parameter sets is proposed based on the performance of previously tried configurations, improving convergence toward an optimal solution. This process helps guard against overfitting while maximizing the model’s predictive skill. The final selected hyperparameters balance model complexity with generalization, ensuring that the model is neither underfit nor excessively tuned

**TABLE 2.** Description of hyperparameters used in the XGBoost model and the selected value using the Bayesian optimization procedure.

Hyperparameter	Explanation	Selected Value
n_estimators	The total number of trees to be built during boosting	184
max_depth	The maximum allowable depth of each decision tree	7
learning_rate	The shrinkage factor that scales each tree’s contribution to prevent overfitting	0.0938
subsample	The fraction of training data sampled (rows) for growing each tree	0.9725
colsample_bytree	The fraction of features (columns) used to build each tree	0.9976
reg_alpha	The L1 regularization penalty applied to leaf weights	0.1412
reg_lambda	The L2 regularization penalty applied to leaf weights	0.0165

to the training data. The selected hyperparameters are shown in Table 2. By learning from a wide array of simulated diurnal conditions and land-cover compositions, the resulting XGBoost model can estimate T2M from LST across a spectrum of urban morphologies and vegetation ratios.

## IV. RESULTS

### A. LST-T2M RELATIONSHIP IN uELM

Figure 2 presents an overview of how T2M and LST are related under the full range of land-cover configurations tested in uELM. In Figure 1a, a high R<sup>2</sup> value (0.82) indicates that the two variables track each other closely overall. The slope of 0.89 ( $\Delta T2M/\Delta LST = 0.89$ ) implies that T2M exhibits a more constrained range than LST, reflecting the effect of atmospheric mixing compared to surface heating. Figure 2b further reveals a clear diurnal dependence, with the slope tending to be lower near dawn and dusk and peaking around midday. This means that the variability of T2M is higher under direct sunlight and the variability of LST is higher during nighttime. This is largely due to differences in how surface materials and the lower atmosphere respond to solar heating and radiative cooling. During the daytime, strong solar heating drives atmospheric mixing, so a small change in LST often produces a relatively larger shift in T2M [43]. By contrast, nighttime conditions are more stable. Thus, surfaces cooling at different rates, causes LST to vary more widely overall while T2M remains comparatively constrained by the slower, more uniform cooling of the lower atmosphere [44], [45].

Figure 2c illustrates how the  $\Delta T2M/\Delta LST$  slope evolves under different land-cover distributions, with each bar segment representing the fraction of land covers. A general trend is that T2M shows more variability compared to LST under more vegetated conditions, especially under conditions with trees. For the urban segments, low-rise buildings tend to increase the slope compared to the mid-rise buildings, but this is very small. This is because in more vegetated

environments, vegetation moderates surface heating and cooling—through shading and evapotranspiration—so LST remains relatively stable. At the same time, T2M can still fluctuate in response to atmospheric processes like advection and boundary-layer mixing, leading to a comparatively larger  $\Delta T2M/\Delta LST$  slope. By contrast, in heavily urbanized settings, the land surface itself often exhibits greater temperature swings (i.e., higher LST variability), which narrows the gap between changes in LST and changes in T2M [46], [47], [48], [49]. It is important to note that some variation may result from the interplay of multiple factors (e.g., hour of the day, moisture availability, surface albedo). Nonetheless, these findings underscore that the type and intensity of urban settings, as well as the presence of vegetation, can markedly influence how LST translates into near-surface air temperature.

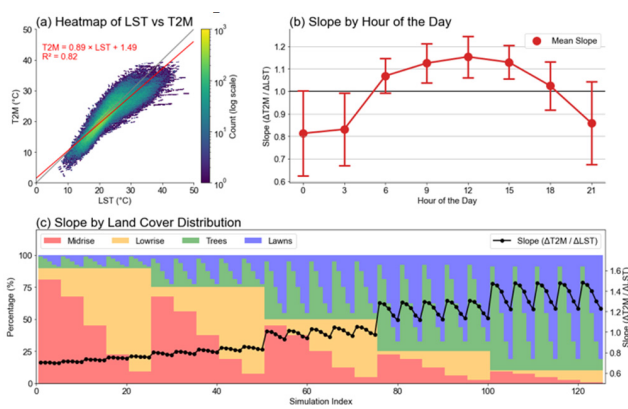


**FIGURE 2.** (a) Heatmap illustrating the relationship between LST (x-axis) and T2M (y-axis) for all 125 uELM simulations. Colors are scaled logarithmically to show data density. (b) Hourly variation of the  $\Delta T2M/\Delta LST$  slope. Error bars denote the range of slope values across all simulations at each hour. (c) Land-cover composition for each of the 125 simulations (x-axis) and the corresponding  $\Delta T2M/\Delta LST$  slope (black line, right y-axis). Each color block indicates the fraction of mid-rise buildings, low-rise buildings, trees, or lawns in a given simulation.

Figure 3 illustrates how, at a fixed T2M, the corresponding LST differs among land-cover types that each occupy more than 75% of a given area. To derive these values, I selected the median T2M at each hour and compared the resulting LST across these dominant land covers. During nighttime, urban areas retain higher LST, reflecting the considerable heat capacity of built materials, which store energy during the day and release it after sunset—a phenomenon often called the nocturnal surface urban heat island [44], [45], [50]. In contrast, daytime heating is mainly driven by direct solar radiation, making the LST–T2M relationship more uniform across land covers [43], [47]. Collectively, these findings underscore how vegetation promotes more effective nighttime surface cooling: while overall T2M may remain similar, non-urban land covers dissipate surface heat faster, highlighting the key role of surface composition in shaping near-surface thermal conditions.

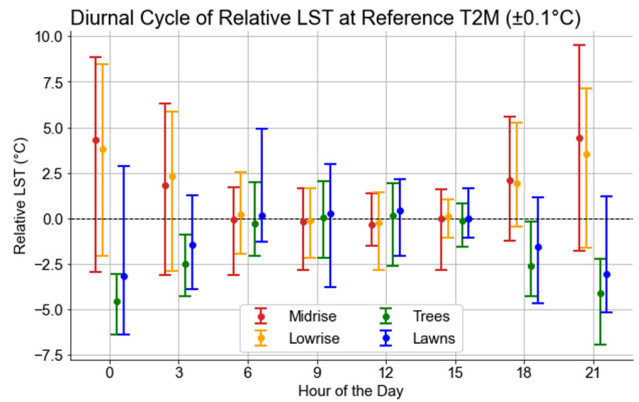


**FIGURE 3.** Relative LST at reference T2M in the uELM simulation. The reference T2M is computed as the hourly median T2M from all simulations, and the relative LST is determined by subtracting this reference T2M from the mean LST in each land-cover scenario. Orange, red, green, and blue symbols represent simulation sets dominated (over 75%) by mid-rise buildings, low-rise buildings, trees, and lawns, respectively. Error bars show the full range of relative LST for each land-cover type at each hour, illustrating the diurnal variation.

**B. COMPARING XGBoost AND uELM BASED T2M ESTIMATION WITH IN-SITU DATA**

From the GOES-16 LST data, it is possible to infer T2M by using XGBoost and uELM driven reverse-engineering method. Figure 4 compares GOES-16 LST, vehicle-measured T2M ( $T2M_{insitu}$ ), and XGBoost/uELM-driven T2M ( $T2M_{ELM}$ ) during two time periods—AF (3–4 pm) and PM (7–8 pm). In the AF timeframe, when incoming solar radiation is still substantial, there is a positive correlation between  $T2M_{insitu}$  and LST (Figure 4a). This relationship becomes even more pronounced when comparing LST to  $T2M_{ELM}$  (Figure 4b), because  $T2M_{ELM}$  is derived from a modeling framework (uELM, further refined by XGBoost) that factors in aggregated land-surface properties over the 2 Km GOES-16 pixel. By contrast, the direct comparison between  $T2M_{insitu}$  and  $T2M_{ELM}$  (Figure 4c) shows a slightly weaker relationship relative to each variable’s correlation with LST. One reason for this discrepancy is the difference in measurement contexts:  $T2M_{insitu}$  originates from mobile sensors mounted on vehicles traveling predominantly along roadways, where localized factors such as asphalt heat storage, traffic congestion, and vehicle exhaust can substantially affect temperature readings. Meanwhile,  $T2M_{ELM}$  represents a grid-average near-surface temperature over a 2 Km cell, incorporating not just roads but also adjacent buildings, vegetated areas, and other land-cover types. Consequently, although both  $T2M_{insitu}$  and  $T2M_{ELM}$  are broadly influenced by solar forcing captured by LST, these distinct sensing domains introduce variances that manifest in the scatter of the data.

In the PM timeframe (Figure 4d–f), the correlations shift significantly, reflecting the complex thermal dynamics that unfold after peak solar input. Figure 4d indicates that the link between LST and  $T2M_{insitu}$  essentially vanishes in the evening, which can be explained by heterogeneous

cooling rates within the urban environment and additional anthropogenic heat sources. After sunset, buildings, roads, and vegetated surfaces release stored heat at different rates, and local conditions—such as traffic volume, engine exhaust, and street-level turbulence—can dominate the roadway environment from which  $T2M_{\text{insitu}}$  is sampled. In contrast, LST and  $T2M_{\text{ELM}}$  (Figure 4e) still exhibit a moderate relationship, though the correlation is weaker than in the afternoon. This residual linkage suggests that the physical parameterizations in uELM, combined with the data-driven corrections from XGBoost, maintain a degree of consistency between surface skin temperature and near-surface air temperature at a coarser 2 Km scale, even as the city transitions to nighttime cooling.

A comparison between  $T2M_{\text{insitu}}$  and  $T2M_{\text{ELM}}$  (Figure 4f) reveals minimal correspondence in the PM. This mismatch emerges because  $T2M_{\text{insitu}}$  is heavily influenced by hyper-local phenomena—vehicles traversing roads that radiate stored heat, localized pockets of air warmed by engines, and intermittent shading from tall buildings. By contrast,  $T2M_{\text{ELM}}$  is grounded in an idealized urban-canyon representation, in which buildings, impervious surfaces, and vegetation are aggregated into a single 2 Km grid cell, preventing the model from fully capturing micro-scale temperature spikes or abrupt cool spots along specific road segments. Consequently, both the small-scale variability in the in-situ measurements and the simplified geometry in the land model led to deviations that become especially pronounced under low solar forcing in the evening.

Nonetheless, the overarching trends indicate that  $T2M_{\text{ELM}}$  and  $T2M_{\text{insitu}}$  each capture meaningful aspects of urban thermal behavior, even though they diverge due to contrasting measurement scales and environmental drivers.

## V. SUMMARY AND DISCUSSIONS

### A. SUMMARY AND KEY FINDINGS

This study employs a hybrid framework that combines a high-resolution, physics-based land model (uELM) and a machine-learning inversion method (XGBoost) to examine how variations in urban–rural fractions, building typologies (mid-rise vs. low-rise), and vegetation (trees vs. lawns) shape the relationship between land surface temperature (LST) and near-surface air temperature ( $T2M$ ).

In total, 125 systematically varied uELM simulations were performed by adjusting the proportions of these land-cover elements in a 1 Km  $\times$  1 Km domain, later aggregated to 2 Km to match GOES-16 satellite retrievals. This modeling setup captures a wide range of urban thermal conditions—encompassing diverse building heights, material properties, and vegetation ratios—and provides an extensive dataset for assessing how changes in land cover affect LST– $T2M$  coupling.

A key result emerging from these simulations is that daytime conditions, particularly in the early afternoon (around 3–4 pm), exhibit a relatively strong correlation

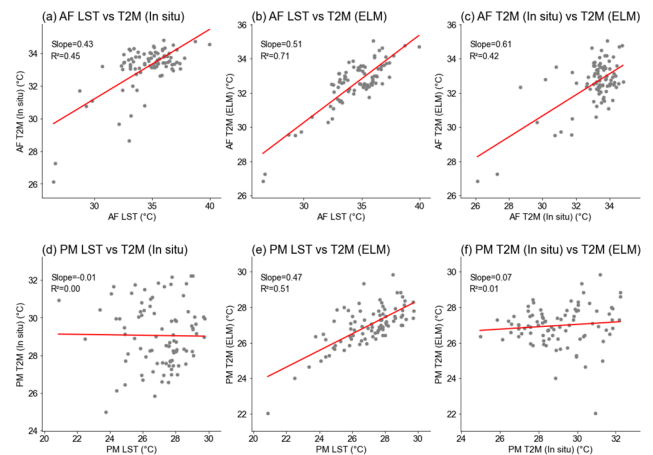


**FIGURE 4.** (a) Scatterplot of GOES-16 LST (x-axis) versus vehicle-measured  $T2M$  ( $T2M_{\text{in-situ}}$ , y-axis) during the afternoon (AF, 3–4 pm) period, with a red linear regression line and corresponding slope and  $R^2$  values as text in upper left. (b) Same time period (AF) but GOES-16 LST (x-axis) compared to XGBoost and uELM-driven  $T2M$  ( $T2M_{\text{ELM}}$ , y-axis), also showing a regression line and slope/ $R^2$ . (c) Comparison of vehicle-measured  $T2M$  ( $T2M_{\text{in-situ}}$ , x-axis) and XGBoost and uELM-driven  $T2M$  ( $T2M_{\text{ELM}}$ , y-axis) for AF, with the linear fit included. (d–f) Same as (a–c), respectively, for the evening (PM, 7–8 pm) period.

between LST and  $T2M$ , driven by intense solar heating and robust boundary-layer mixing. In contrast, the evening period (7–8 pm) reveals more complex dynamics: surfaces such as roads, walls, and roofs release stored heat at varying rates, causing LST to diverge from  $T2M$ . While simulations show a general drop in both LST and  $T2M$  after sunset, local micro-scale processes—such as radiative trapping within street canyons and residual heat retained by impervious surfaces—can create significant spatial heterogeneity in how  $T2M$  and LST decouple. Notably, the presence of vegetation tends to moderate the diurnal extremes by limiting daytime surface heating (through shading) and enhancing nighttime cooling (via evapotranspiration), whereas heavily urbanized grid cells exhibit stronger nighttime LST retention.

Beyond these direct uELM simulations, an innovative facet of this work is the “reverse-engineering” of  $T2M$  from LST by using the model-generated  $T2M$ –LST pairs as a training dataset for eXtreme Gradient Boosting (XGBoost). Rather than relying solely on simple statistical correlations, this approach leverages the physics-based realism of uELM to learn how land-cover configuration and diurnal cycles jointly govern the translation from LST to  $T2M$ . The resulting XGBoost model is then tested against in-situ  $T2M$  measurements collected by vehicle-based sensors traversing the Chicago area. Afternoon comparisons show that  $T2M_{\text{insitu}}$  aligns relatively well with both GOES-16 LST and XGBoost-derived  $T2M$ , reflecting stronger atmospheric mixing and more uniform solar forcing across the domain. By contrast, evening comparisons reveal discrepancies, highlighting the difficulty of representing hyperlocal road-level temperatures and anthropogenic heat sources—particularly

in an aggregated 2 Km modeling framework that simplifies real-world street canyons.

Altogether, these findings illustrate the dual importance of diurnal forcing and urban morphology in mediating the LST–T2M linkage and demonstrate the utility of combining a validated land model with a data-driven inversion technique to extend T2M estimates to large spatial domains.

## B. DISCUSSIONS

By systematically analyzing the interactions among LST, T2M, urban fraction, and vegetation cover, this study contributes several key insights with direct implications for urban climate research and practical planning. The systematic variation of building heights (mid-rise vs. low-rise) and vegetation (trees vs. lawns) clarifies how different urban morphologies govern daytime heating and nighttime cooling. This modeling approach elucidates the roles of shading, evapotranspiration, and material thermal inertia, which can aid city planners in designing effective heat-mitigation strategies—such as increasing tree canopy in highly built-up areas or modifying building materials to reduce daytime surface heating. Merging physics-based simulations (uELM) with a machine-learning inversion (XGBoost) moves beyond simple empirical LST–T2M conversions, allowing robust near-surface temperature fields to be generated from satellite LST while accounting for diurnal cycles and land-cover variability. This capability is particularly advantageous for large metropolitan regions where dense in-situ weather station data may be limited.

Comparisons between  $T2M_{\text{insitu}}$  and  $T2M_{\text{ELM}}$  underscore the scaling challenges inherent in urban climatology. Vehicle-based measurements capture hyperlocal conditions that can differ substantially from the 1–2 Km resolution patterns represented by the model. Recognizing how these scales align or diverge is crucial when reconciling intensive field campaigns with broader climate assessments. As cities worldwide confront intensifying heat waves and urban heat island (UHI) effects, the findings also demonstrate that heterogeneous land covers—varying mixes of building types and vegetation—can produce distinct temperature outcomes. Inverting satellite LST to obtain T2M through physically grounded relationships supports decision-makers who need high-resolution temperature maps to identify at-risk zones and prioritize interventions such as urban greening, reflective roofing, or strategically placed parks. This hybrid approach is therefore novel in spanning a wide array of land-cover attributes, systematically learning T2M–LST relationships, and validating them rigorously against in-situ data. Although discrepancies between  $T2M_{\text{insitu}}$  and  $T2M_{\text{ELM}}$  during evening hours highlight the importance of micro-scale processes, the overarching trends indicate that this framework can be adapted for real-time urban heat monitoring across diverse regions.

Despite these promising findings, several limitations and sources of uncertainty remain, along with avenues for further development. The idealized urban canyon representation

in uELM is designed to capture essential urban thermodynamics but omits finer details such as street-by-street width variations, building footprints, anthropogenic heat sources, and the diverse thermal properties of materials. These oversimplifications can become especially problematic at night, when local variations in heat retention lead to pronounced temperature gradients that are not fully resolved by coarser models. Measurement scale disparities further complicate this issue: while  $T2M_{\text{ELM}}$  is generated at 1 Km resolution and aggregated to 2 Km for GOES-16 LST comparisons,  $T2M_{\text{insitu}}$  captures hyperlocal road-level phenomena. Additionally, the study uses default urban and vegetation parameter values rather than a region-specific parameterization calibrated to Chicago’s buildings, plant species, and municipal infrastructure. Observational limitations also arise from cloud-induced gaps in satellite data and the relatively short duration of vehicle-based campaigns, restricting opportunities for validation.

Future work can address these constraints by incorporating building-level heat release and anthropogenic emissions in uELM and refining the street-canyon representation. Employing multi-layer urban canopy models or sub-grid-scale parameterizations could approximate real-world building arrangements and traffic emissions more accurately, narrowing the gap between  $T2M_{\text{insitu}}$  and  $T2M_{\text{ELM}}$  in nocturnal conditions. Linking uELM to advanced mesoscale atmospheric models would further illuminate the interplay between local urban canyons and the regional boundary layer. The realism of meteorological inputs can be improved by incorporating higher-resolution reanalysis datasets or denser observational networks, and data assimilation methods that continuously update model states using in-situ and satellite measurements could reduce discrepancies during evening cooling.

Although the current focus is on Chicago, the approach is transferable to other cities, including those with distinct climates or architecture. Integrating additional satellite LST products such as MODIS, VIIRS, or Sentinel can expand the temporal and spatial coverage, broadening the model’s applicability to other regions and supporting city-scale planning and climate adaptation. As climate change intensifies extreme heat events, the ability to invert LST into T2M at fine resolution could serve as a practical tool for identifying hotspots, evaluating interventions to mitigate UHI effects, and informing public health strategies.

Scenario-based simulations that combine uELM and XGBoost may help local officials assess the potential effects of adopting cool-roof technologies, increasing urban green space, or implementing building-energy retrofits on near-surface thermal conditions. Recent studies underscore the rising importance of cross-disciplinary collaboration, uniting climate science, machine learning, and policy frameworks to develop resilient urban environments [51], [52], [53]. Extending this hybrid modeling approach with more detailed socio-economic data and exposure metrics will likely strengthen urban resilience planning under future climate scenarios.

Ultimately, by fusing physics-based realism with data-driven analytics, the study offers a promising pathway for refining both operational T2M retrievals and long-term urban heat management strategies in an increasingly warming world.

## REFERENCES

- [1] J. Lee and A. E. Dessler, "Future temperature-related deaths in the U.S.: The impact of climate change, demographics, and adaptation," *GeoHealth*, vol. 7, no. 8, 2023, Art. no. e2023GH000799.
- [2] C. Heaviside, H. Macintyre, and S. Vardoulakis, "The urban heat island: Implications for health in a changing environment," *Current Environ. Health Rep.*, vol. 4, no. 3, pp. 296–305, Sep. 2017.
- [3] J. Tan, Y. Zheng, X. Tang, C. Guo, L. Li, G. Song, X. Zhen, D. Yuan, A. J. Kalkstein, F. Li, and H. Chen, "The urban heat island and its impact on heat waves and human health in Shanghai," *Int. J. Biometeorol.*, vol. 54, no. 1, pp. 75–84, Jan. 2010.
- [4] J. Lee and A. E. Dessler, "The impact of neglecting climate change and variability on ERCOT's forecasts of electricity demand in Texas," *Weather, Climate, Soc.*, vol. 14, no. 2, pp. 499–505, 2022.
- [5] X. Li, Y. Zhou, S. Yu, G. Jia, H. Li, and W. Li, "Urban heat island impacts on building energy consumption: A review of approaches and findings," *Energy*, vol. 174, pp. 407–419, May 2019.
- [6] A. J. Arnfield, "Two decades of urban climate research: A review of turbulence, exchanges of energy and water, and the urban heat island," *Int. J. Climatol., J. Roy. Meteorol. Soc.*, vol. 23, no. 1, pp. 1–26, Jan. 2003.
- [7] Y. Sun and G. Augenbroe, "Urban heat island effect on energy application studies of office buildings," *Energy Buildings*, vol. 77, pp. 171–179, Jul. 2014.
- [8] Y. Cui, M. Yin, X. Cheng, J. Tang, and B.-J. He, "Towards cool cities and communities: Preparing for an increasingly hot future by the development of heat-resilient infrastructure and urban heat management plan," *Environ. Technol. Innov.*, vol. 34, May 2024, Art. no. 103568.
- [9] H. Saaroni, J. H. Amorim, J. A. Hiemstra, and D. Pearlmutter, "Urban green infrastructure as a tool for urban heat mitigation: Survey of research methodologies and findings across different climatic regions," *Urban Climate*, vol. 24, pp. 94–110, Jun. 2018.
- [10] X. Zhou and H. Chen, "Impact of urbanization-related land use land cover changes and urban morphology changes on the urban heat island phenomenon," *Sci. Total Environ.*, vol. 635, pp. 1467–1476, Sep. 2018.
- [11] S. Chapman, J. E. M. Watson, A. Salazar, M. Thatcher, and C. A. McAlpine, "The impact of urbanization and climate change on urban temperatures: A systematic review," *Landscape Ecol.*, vol. 32, no. 10, pp. 1921–1935, Oct. 2017.
- [12] H. Feng, X. Zhao, F. Chen, and L. Wu, "Using land use change trajectories to quantify the effects of urbanization on urban heat island," *Adv. Space Res.*, vol. 53, no. 3, pp. 463–473, Feb. 2014.
- [13] T. Chakraborty and Y. Qian, "Urbanization exacerbates continental-to regional-scale warming," *One Earth*, vol. 7, no. 8, pp. 1387–1401, Aug. 2024.
- [14] Y. Yu and P. Yu, "Land surface temperature product from the GOES-R series," in *The GOES-R Series*. Amsterdam, The Netherlands: Elsevier, 2020, pp. 133–144.
- [15] Y. Yu, D. Tarpley, J. L. Privette, M. D. Goldberg, M. K. R. V. Raja, K. Y. Vinnikov, and H. Xu, "Developing algorithm for operational GOES-R land surface temperature product," *IEEE Trans. Geosci. Remote Sens.*, vol. 47, no. 3, pp. 936–951, Mar. 2009.
- [16] T. N. Phan and M. Kappas, "Application of MODIS Land Surface Temperature data: A systematic literature review and analysis," *J. Appl. Remote Sens.*, vol. 12, no. 4, Oct. 2018, Art. no. 041501.
- [17] Z. Wan, "New refinements and validation of the MODIS land-surface temperature/emissivity products," *Remote Sens. Environ.*, vol. 112, no. 1, pp. 59–74, Jan. 2008.
- [18] A. Benali, A. C. Carvalho, J. P. Nunes, N. Carvalhais, and A. Santos, "Estimating air surface temperature in Portugal using MODIS LST data," *Remote Sens. Environ.*, vol. 124, pp. 108–121, Sep. 2012.
- [19] M. P. Cresswell, A. P. Morse, M. C. Thomson, and S. J. Connor, "Estimating surface air temperatures, from Meteosat land surface temperatures, using an empirical solar zenith angle model," *Int. J. Remote Sens.*, vol. 20, no. 6, pp. 1125–1132, Jan. 1999.
- [20] S. A. Shiflett, L. L. Liang, S. M. Crum, G. L. Feyisa, J. Wang, and G. D. Jenerette, "Variation in the urban vegetation, surface temperature, air temperature Nexus," *Sci. Total Environ.*, vol. 579, pp. 495–505, Feb. 2017.
- [21] J. Cao, W. Zhou, Z. Zheng, T. Ren, and W. Wang, "Within-city spatial and temporal heterogeneity of air temperature and its relationship with land surface temperature," *Landscape Urban Planning*, vol. 206, Feb. 2021, Art. no. 103979.
- [22] B. Bechtel, K. Zakšek, J. Oßenbrügge, G. Kaveckis, and J. Böhner, "Towards a satellite based monitoring of urban air temperatures," *Sustain. Cities Soc.*, vol. 34, pp. 22–31, Oct. 2017.
- [23] M. Urban, J. Eberle, C. Hüttich, C. Schullius, and M. Herold, "Comparison of satellite-derived land surface temperature and air temperature from meteorological stations on the pan-arctic scale," *Remote Sens.*, vol. 5, no. 5, pp. 2348–2367, May 2013.
- [24] A. S. Alqasemi, M. E. Hereher, A. M. F. Al-Quraishi, H. Saibi, A. Aldahan, and A. Abuelgasim, "Retrieval of monthly maximum and minimum air temperature using MODIS Aqua land surface temperature data over the United Arab Emirates," *Geocarto Int.*, vol. 37, no. 10, pp. 2996–3013, May 2022.
- [25] R. S. Dos Santos, "Estimating spatio-temporal air temperature in London (U.K.) using machine learning and Earth observation satellite data," *Int. J. Appl. Earth Observ. Geoinf.*, vol. 88, Jun. 2020, Art. no. 102066.
- [26] L. Zhou, F. Huo, R. Cai, H. Chen, and L. Xu, "Improved temperature prediction using deep residual networks in Hunan province, China," *Meteorol. Atmos. Phys.*, vol. 136, no. 4, pp. 1–14, Jul. 2024.
- [27] M. Yu, F. Xu, W. Hu, J. Sun, and G. Cervone, "Using long short-term memory (LSTM) and Internet of Things (IoT) for localized surface temperature forecasting in an urban environment," *IEEE Access*, vol. 9, pp. 137406–137418, 2021.
- [28] J. Chung, Y. Lee, W. Jang, S. Lee, and S. Kim, "Correlation analysis between air temperature and MODIS land surface temperature and prediction of air temperature using TensorFlow long short-term memory for the period of occurrence of cold and heat waves," *Remote Sens.*, vol. 12, no. 19, p. 3231, Oct. 2020.
- [29] T. T. K. Tran, S. M. Bateni, S. J. Ki, and H. Vosoughifar, "A review of neural networks for air temperature forecasting," *Water*, vol. 13, no. 9, p. 1294, May 2021.
- [30] J. Hrisko, P. Ramamurthy, Y. Yu, P. Yu, and D. Melecio-Vázquez, "Urban air temperature model using GOES-16 LST and a diurnal regressive neural network algorithm," *Remote Sens. Environ.*, vol. 237, Feb. 2020, Art. no. 111495.
- [31] F. Salamanca, A. Martilli, M. Tewari, and F. Chen, "A study of the urban boundary layer using different urban parameterizations and high-resolution urban canopy parameters with WRF," *J. Appl. Meteorol. Climatol.*, vol. 50, no. 5, pp. 1107–1128, May 2011.
- [32] D. Zhu and R. Ooka, "WRF-based scenario experiment research on urban heat island: A review," *Urban Climate*, vol. 49, May 2023, Art. no. 101512.
- [33] K. W. Oleson and J. Feddema, "Parameterization and surface data improvements and new capabilities for the community land model urban (CLMU)," *J. Adv. Model. Earth Syst.*, vol. 12, no. 2, p. 2018, Feb. 2020.
- [34] D. M. Lawrence et al., "The community land model version 5: Description of new features, benchmarking, and impact of forcing uncertainty," *J. Adv. Model. Earth Syst.*, vol. 11, no. 12, pp. 4245–4287, Oct. 2019.
- [35] G. B. Bonan, K. W. Oleson, M. Vertenstein, S. Levis, X. Zeng, Y. Dai, R. E. Dickinson, and Z. Yang, "The land surface climatology of the community land model coupled to the NCAR community climate model," *J. Climate*, vol. 15, no. 22, pp. 3123–3149, Oct. 2002.
- [36] U. P. Bhautmage, J. C. H. Fung, J. Pleim, and M. M. F. Wong, "Development and evaluation of a new urban parameterization in the weather research and forecasting (WRF) model," *J. Geophys. Research: Atmos.*, vol. 127, no. 16, p. 2021, Aug. 2022.
- [37] F. Yuan, D. Wang, S.-C. Kao, M. Thornton, D. Ricciuto, V. Salmon, C. Iversen, P. Schwartz, and P. Thornton, "An ultrahigh-resolution E3SM land model simulation framework and its first application to theeward peninsula in Alaska," *J. Comput. Sci.*, vol. 73, Nov. 2023, Art. no. 102145.
- [38] F. Yuan et al., "An ultrahigh-resolution E3SM land model simulation framework and its first application to the Seward Peninsula in Alaska," *J. Comput. Sci.*, vol. 73, 2023, Art. no. 102145. [Online]. Available: <https://www.sciencedirect.com/science/article/abs/pii/S187750323002053>
- [39] D. Wang, P. Schwartz, F. Yuan, P. Thornton, and W. Zheng, "Toward ultrahigh-resolution E3SM land modeling on exascale computers," *Comput. Sci. Eng.*, vol. 24, no. 6, pp. 44–53, Nov. 2022.

- [40] Y. Yu, D. Tarpley, J. L. Privette, L. E. Flynn, H. Xu, M. Chen, K. Y. Vinnikov, D. Sun, and Y. Tian, "Validation of GOES-R satellite land surface temperature algorithm using SURFRAD ground measurements and statistical estimates of error properties," *IEEE Trans. Geosci. Remote Sens.*, vol. 50, no. 3, pp. 704–713, Mar. 2011.
- [41] NOAA. *Coastal Change Analysis Program (C-CAP) High-Resolution Land Cover*. Accessed: Dec. 15, 2024. [Online]. Available: <https://www.coast.noaa.gov/htdata/raster1/landcover/bulkdownload/hires/>
- [42] T. Chen and C. Guestrin, "XGBoost: A scalable tree boosting system," in *Proc. 22nd ACM SIGKDD Int. Conf. Knowl. Discovery Data Mining*, Aug. 2016, pp. 785–794.
- [43] J. Lai, W. Zhan, F. Huang, J. Voogt, B. Bechtel, M. Allen, S. Peng, F. Hong, Y. Liu, and P. Du, "Identification of typical diurnal patterns for clear-sky climatology of surface urban heat islands," *Remote Sens. Environ.*, vol. 217, pp. 203–220, Nov. 2018.
- [44] J. Lai, W. Zhan, J. Voogt, J. Quan, F. Huang, J. Zhou, B. Bechtel, L. Hu, K. Wang, C. Cao, and X. Lee, "Meteorological controls on daily variations of nighttime surface urban heat islands," *Remote Sens. Environ.*, vol. 253, Feb. 2021, Art. no. 112198.
- [45] S. Peng, S. Piao, P. Ciais, P. Friedlingstein, C. Ottle, F.-M. Bréon, H. Nan, L. Zhou, and R. B. Myneni, "Surface urban heat island across 419 global big cities," *Environ. Sci. Technol.*, vol. 46, no. 2, pp. 696–703, Jan. 2012.
- [46] A. Kumar, M. Mukherjee, and A. Goswami, "Inter-seasonal characterization and correlation of surface urban heat island (SUHI) and canopy urban heat island (CUHI) in the urbanized environment of Delhi," *Remote Sens. Appl., Soc. Environ.*, vol. 30, Apr. 2023, Art. no. 100970.
- [47] Y. Hu, M. Hou, G. Jia, C. Zhao, X. Zhen, and Y. Xu, "Comparison of surface and canopy urban heat islands within megacities of eastern China," *ISPRS J. Photogramm. Remote Sens.*, vol. 156, pp. 160–168, Oct. 2019.
- [48] P. Shen, S. Zhao, D. Zhou, B. Lu, Z. Han, Y. Ma, Y. Wang, C. Zhang, C. Shi, L. Song, Z. Pan, Z. Li, and S. Liu, "Surface and canopy urban heat island disparities across 2064 urban clusters in China," *Sci. Total Environ.*, vol. 955, Dec. 2024, Art. no. 177035.
- [49] H. Du, W. Zhan, J. Voogt, B. Bechtel, T. C. Chakraborty, Z. Liu, L. Hu, Z. Wang, J. Li, P. Fu, W. Liao, M. Luo, L. Li, S. Wang, F. Huang, and S. Miao, "Contrasting trends and drivers of global surface and canopy urban heat islands," *Geophys. Res. Lett.*, vol. 50, no. 15, Aug. 2023, Art. no. e2023GL104661.
- [50] J. Lee, "Assessment of U.S. urban surface temperature using GOES-16 and GOES-17 data: Urban heat Island and temperature inequality," *Weather, Climate, Soc.*, vol. 16, no. 2, pp. 315–329, Apr. 2024.
- [51] Y. Cheng, L. Zhao, T. Chakraborty, K. W. Oleson, M. Demuzere, X. Liu, Y. Che, W. Liao, Y. Zhou, and X. Li, "U-Surf: A Global 1 km spatially continuous urban surface property dataset for kilometer-scale urban-resolving Earth system modeling," *Earth Syst. Sci. Data Discuss.*, vol. 2024, pp. 1–38, Oct. 2024.
- [52] R. I. McDonald, T. Biswas, T. C. Chakraborty, T. Kroeger, S. C. Cook-Patton, and J. E. Fargione, "Current inequality and future potential of U.S. urban tree cover for reducing heat-related health impacts," *NPJ Urban Sustainability*, vol. 4, no. 1, p. 18, Apr. 2024.
- [53] T. Chakraborty, T. Biswas, L. S. Campbell, B. Franklin, S. S. Parker, and M. Tukman, "Feasibility of afforestation as an equitable nature-based solution in urban areas," *Sustain. Cities Soc.*, vol. 81, Jun. 2022, Art. no. 103826.



**JANGHO LEE** received the B.S. degree in earth and environmental sciences from Seoul National University, Seoul, South Korea, in 2018, and the Ph.D. degree in atmospheric sciences from Texas A&M University, College Station, TX, USA, in 2023.

Since 2023, he has been a Postdoctoral Researcher with the University of Illinois at Chicago as a part of the Community Research on Climate and Urban Science (CROCUS) Project.

His research interests include climate informatics, statistical climatology, deep learning, remote sensing, climate impacts, and land-atmospheric modeling.

Dr. Lee has been a member of American Geophysical Union (AGU) and American Meteorological Society (AMS), since 2018.

• • •